https://doi.org/10.5194/egusphere-2024-3601
Preprint. Discussion started: 16 December 2024

Strong aerosol indirect radiative effect from dynamic-driven diurnal variations of cloud water adjustments

Jiayi Li[1]†, Yang Wang[1]†, Jiming Li[1*], Weiyuan Zhang[1], Lijie Zhang[1], Yuan Wang[1]

[1] Collaborative Innovation Center for Western Ecological Safety, College of Atmospheric Sciences, Lanzhou University, Lanzhou 730000, China.

Correspondence to: Jiming Li (lijiming@lzu.edu.cn)

† These authors contributed equally to this work.

Abstract. Aerosol-cloud interaction (ACI) is the critical yet most uncertain process in future climate projections. A major challenge is the sign and magnitude of cloud liquid water path (LWP) response to aerosol perturbations (represented by cloud droplet number concentration, N_d) at different temporal and spatial scales are highly variable, but potential microphysical-dynamical mechanisms are still unclear, especially at a diurnal scale. Here, robust observational evidence from geostationary satellite reveals that the diurnal variation of LWP adjustments is driven primarily by diurnal-related boundary layer decoupling and cloud-top entrainment. Strikingly, these diurnal adjustments exhibit a distinct regional pattern associated with cloud regimes. We find that the cooling effect of LWP adjustments would be underestimated by up to 86% in study regions if neglecting their diurnal variations, leading to a further 45% offset of Twomey effect, thus biasing aerosol indirect effect toward a warming direction. Our findings highlight the key role of diurnal variation of ACI in reducing the uncertainty in climate projections.

1 Introduction

Marine low-level clouds (MLCs), which cover one-third part of the global ocean (Klein and Hartmann, 1993), exert a strong cooling effect by reflecting the incoming solar radiation back into space with little impact on the outgoing longwave radiation (Jiang et al., 2023). Their reflectivity to solar radiation is highly sensitive to atmospheric aerosol concentrations because aerosols can serve as the cloud condensation nuclei (CCN) to modify the mediated variables of aerosol-cloud interactions (ACI) (e.g. droplet number concentrations, N_d; effective radius, r_e). While the cooling effect of ACI may partly offset the global warming induced by greenhouse gases, ACI still contributes the largest uncertainty of aerosol radiative forcing and future climate projections. Aerosol-induced increases in CCN can enhance N_d and hence reduce r_e, boosting cloud albedo while holding cloud liquid water content (the Twomey effect) (Twomey, 1977), which is the instantaneous radiative forcing from ACI (RF_{aci}). In addition to Twomey effect, changes in cloud macrophysical properties induced by aerosol variations lead to further alterations in cloud albedo, it is called rapid adjustments (e.g., LWP adjustments) (Bellouin et al., 2020). While the Twomey effect is well-recognized, however, LWP adjustments are highly uncertain as the least understanding and most poorly

https://doi.org/10.5194/egusphere-2024-3601
Preprint. Discussion started: 16 December 2024

quantified in all climate forcing (IPCC, 2023). LWP adjustments exhibit not only large spatiotemporal variability (Gryspeerdt et al., 2019, 2022a; Han et al., 2002; Michibata et al., 2016) but also bidirectional sign. For example, it has been documented that liquid water path (LWP) can either increase due to precipitation suppression (positive LWP adjustments) (Albrecht, 1989) or decrease due to entrainment-drying (negative LWP adjustments) (Ackerman et al., 2004; Bretherton et al., 2007; Small et al., 2009). These large uncertainties in LWP adjustments are possibly attributed to the complex interplay of microphysical-dynamical conditions and aerosol loading (represented by N_d) that vary with different temporal and spatial scales (Bender et al., 2019; Chen et al., 2014; Glassmeier et al., 2021; Gryspeerdt et al., 2022a).

Numerous observational studies have been carried out to understand the extent of this variability and uncertainties of LWP adjustments, with the aim of constraining model simulations (Gryspeerdt et al., 2019, 2021; Rosenfeld et al., 2019; Trofimov et al., 2020; Wilcox, 2010). These investigations have spanned various regions and targets, revealing diverse cloud responses attributable to the varied mechanisms of LWP adjustments. Meanwhile, it has been confirmed that the uncertainty source of LWP adjustments refers to various factors such as analysis methods, sampling strategies, meteorology covariations (Chen et al., 2014; Gryspeerdt et al., 2022b; Rosenfeld et al., 2019, 2023). Here, we focus on the time-dependence of LWP adjustments (that is, diurnal variations) as it is associated with both sampling strategies and meteorology covariations. Actually, it has been established that marine cloud properties and cloud-topped marine boundary layer exhibit prominent diurnal variations in response to solar radiation, which are closely related to their regional dependence (Duynkerke and Hignett, 1993; Wood et al., 2002). The microphysical-dynamical boundary layer feedback, which generally covaries with regional diurnal cycle, could augment or weaken the LWP adjustments and thus lead to the diurnal variation of LWP adjustments with broad spreads and even different signs. This means that a one-size-fits-all approach to global-mean LWP adjustments may not provide a robust constraint, given the regional and temporal mechanisms at play (Michibata et al., 2016).However, the microphysical-dynamical mechanisms behind are complex and still poorly understood (Feingold et al., 2024). This drives the conclusion that the diurnal variations of LWP adjustments could be one of the most significant yet overlooked sources of uncertainty of ACI.

However, to date a majority of researches have relied on observations from polar-orbiting satellites to investigate the spatial distribution and long-term variations of N_d due to limitations of observational techniques (Bennartz and Rausch, 2017; Li et al., 2018; McCoy et al., 2018). These methods are insufficient to depict the time-dependence nature of LWP adjustments. Based on Himawari-8 geostationary satellite, this work demonstrates that diurnal variations of LWP adjustments in two typical regions are primarily driven by diurnal-related boundary layer decoupling and cloud-top entrainment, leading to large underestimation of the cooling effect. These results expand our understanding regarding the diurnal variations of LWP adjustments, further confirming that this is a significant, yet commonly overlooked, source of uncertainty.

2 Data and Methods

Our analysis focuses on 1° × 1° non-precipitation marine low-level cloud samples, aggregated from filtered pixel-level

https://doi.org/10.5194/egusphere-2024-3601
Preprint. Discussion started: 16 December 2024

satellite data, try to avoid the impact of precipitation on retrieval of N_d and focusing only on the development of clouds in response to aerosol loading associated with microphysical-dynamical conditions over two selected regions. One is located in the west of Australia (25º-35ºS, 95º-105ºE, AUW). The other is in East China Sea (20º-30ºN, 120º-130ºE, ECS), as shown in Figure S1 in Supplementary Materials.

2.1 N_d retrieval based on geostationary satellite product

In this study, 4 years (2016-2019) of hourly cloud microphysical properties data from the Satellite Cloud and Radiation Property retrieval System (SatCORPS) Clouds and the Earth's Radiant Energy System (CERES) Geostationary Satellite (GEO) Edition 4 Himawari-8 over the Northern Hemisphere (NH) (Southern Hemisphere (SH)) Version 1.2 data product (CER_GEO_ED4_HIM08_NH_V01.2, CER_GEO_ED4_HIM08_SH_V01.2) are collected (NASA/LARC/SD/ASDC, 2018b, a). The datasets are derived from the Advanced Himawari Imagers (AHI) on Himawari-8 geostationary satellite, using the Langley Research Center (LARC)s SatCORPS algorithms in support of CERES project (Minnis et al., 2021; Trepte et al., 2019). The retrievals are at 4-km resolution (at nadir) and are sub-sampled to 8 km in NH (6 km in SH). The cloud optical thickness (CLOT), cloud effective radius (r_e) and cloud-top temperature (CLTT) from SatCORPS product during the daytime are used to retrieve N_d in our study. Other cloud properties such as cloud-top height (CLTH), cloud base height (CLBH) and cloud thickness (H) are used in further analysis. The SatCORPS is based on the CERES Ed4 cloud retrieval algorithm with more accurate CLTH and H parameterization (Minnis et al., 2021).

The SatCORPS retrievals provided cloud effective radius (r_e) in 3.9 μm near-infrared band (Kang et al., 2021), which is closest to the cloud top and leads to less bias in further calculation of N_d (Grosvenor et al., 2018). Both N_d and LWP are derived under the adiabatic assumption, described as linear enhancement of liquid water content and constant cloud number concentration from cloud base to top (Bennartz, 2007). N_d can be estimated as:

$$N_d = \frac{\sqrt{5}}{2\pi k}\left(\frac{f_{ad} c_\omega \tau}{Q \rho_w {r_e}^5}\right)^{\frac{1}{2}} \quad (1)$$

where τ represents cloud optical depth and ρ_w is liquid water density. The extinction efficiency $Q \approx 2$, as Q relies less on size parameter in near infrared. k, related to droplet size distribution, is set as 0.8 for maritime cloud (Martin et al., 1994; Painemal and Zuidema, 2011). c_w represents the condensation rate determined by temperature in cloud (here is cloud-top temperature from SatCORPS). A constant adiabatic value (f_{ad}) of 0.8 is used. LWP from SatCORPS is calculated as $\frac{5}{9}\rho_w \tau r_e$. (Li et al., 2018) demonstrated that passive satellite retrievals based on the adiabatic model exhibit strong consistency with active satellite retrievals. Additionally, the SatCORPS Himawari-8 retrievals agree well with in-situ observations according to Kang et al. (2021). The adiabatic model is the most common method to derive N_d from passive satellite observations (Bennartz, 2007; Bennartz and Rausch, 2017; Li et al., 2018; McCoy et al., 2018) and has been validated as a reliable technique for observing changes in long-term variations of N_d (Boers et al., 2006).

Following previous studies (Grosvenor et al., 2018; Gryspeerdt et al., 2019; Li et al., 2018), several sampling strategies

https://doi.org/10.5194/egusphere-2024-3601
Preprint. Discussion started: 16 December 2024

are adopted on cloud pixels to meet the assumption. Only pixels in liquid phase with cloud-top temperature warmer than 268 K under 3.2 km were included. The lower bounds of r_e and τ are set as 4 μm and 4 to reduce uncertainties. Moreover, pixels with solar zenith angle larger than 65° are excluded. Filtered data will be used to calculate N_d and then aggregated to 1° × 1° grid. Each grid contains at least 30 pixels and is considered as a cloud sample.

We followed the previous methods to filter cloud pixels. But this classification only limits cloud top properties and cloud phase, inevitably including different cloud regimes, such as low-level cumulus clouds. This will introduce uncertainties because cumulus clouds and stratocumulus clouds have different adiabatic properties but we have set the adiabatic lapse rate as a constant value in retrieval process. Note that the choices of constant k and f_{ad} may introduce bias into the retrieval of N_d. Studies have found that k parameter varied with the height within cloud and cloud types (Brenguier et al., 2011; Martin et al., 1994; Painemal and Zuidema, 2011). Also, uncertainties may occur as f_{ad} varies with cloud depth (Grosvenor et al., 2018; Min et al., 2012). As acquiring hourly f_{ad} on a global scale is difficult, to date, studies investigating diurnal variations based geostationary satellites continue to employ constant f_{ad} value (Fons et al., 2023; Qiu et al., 2024; Smalley et al., 2024). Since the bias caused by the retrieval contributes equally in all samples, which may change the magnitude of variables without changing the diurnal patterns or the mechanism behind them. Consequently, the uncertainties associated with the aforementioned data will not greatly affect the conclusions of this paper.

In order to minimize the influence of precipitation, particularly the bias introduced in N_d and LWP retrievals due to invalidating the adiabatic assumption, only non-precipitating clouds are discussed in this study. Therefore, cloud samples are subject to strict precipitation criterion. Besides the classical threshold $r_e < 14$ μm (Rosenfeld et al., 2012), GPM IMERG Final Precipitation L3 Half Hourly 0.1 degree x 0.1 degree V07 (GPM_3IMERGHH) is also used as an auxiliary judgment (Huffman et al., 2020). The double-check is applied since there are distinct elements that do not overlap of the two criteria. To align these two satellite products, SatCORPS cloud pixels within each 0.1° grid of GPM_3IMERGHH are assigned the same precipitation value. Cloud samples are regarded as non-precipitation only if the averaged effective radius is under 14 μm and GPM_3IMERGHH precipitation rate equals 0 mm/hr in 1° × 1° grid. In total, we collect 246762 cloud samples in AUW and 161581 cloud samples in ECS using 4-year (2016-2019) hourly record from SatCORPS Himawari-8.

2.2 Quantification of LWP adjustments

To quantify LWP response, both direct and indirect methods have been used in previous studies. The logarithmic relationship between N_d and LWP ($\frac{\partial \ln LWP}{\partial \ln N_d}$) is a direct way to quantify LWP sensitivity to aerosol perturbations, where N_d is considered as a proxy of CCN. Another indirect way describing the variation of cloud water due to aerosols ($-\frac{\Delta \ln \tau}{\Delta \ln r_e}$) is deduced from the contributions of changes in LWP and r_e to the changes in cloud optical depth ($\frac{\Delta \tau}{\tau} = \frac{\Delta LWP}{LWP} - \frac{\Delta r_e}{r_e}$) (Christensen and Stephens, 2011; Coakley and Walsh, 2002). Whereas the latter method is put forward with a default condition that Δr_e is always negative, it is only applicable to small-scale pollution tracks like industry tracks, volcano tracks or ship tracks etc. (Rahu et al.,

https://doi.org/10.5194/egusphere-2024-3601
Preprint. Discussion started: 16 December 2024

2022; Toll et al., 2019). Therefore, the former method is applied in this study, which has been commonly used in researches of aerosol-cloud interactions based on large-scale satellite observations (Glassmeier et al., 2021; Gryspeerdt et al., 2019; Rosenfeld et al., 2019).

LWP adjustment at any given moment is the result of all available data at that moment. The regression slope of N_d and LWP in log-log space ($\frac{\partial \ln LWP}{\partial \ln N_d}$) is calculated on 1° grid scale. Following previous studies (Fons et al., 2023; Rosenfeld et al., 2019), we choose the median LWP in each ln(N_d) bin as the feature point for the entire sample space making the regression more representative of the overall characteristics of the samples (black dots in Figure 1, A and D). Since the relationship between N_d and LWP in non-precipitation clouds shows a non-linear trend, turning points in N_d are found to characterize LWP adjustments in different N_d stages (green, purple and blue lines in Figure 1, A and D). In AUW region (Figure 1A), the highest point before 100 cm^{-3} and the lowest point between 100 and 300 cm^{-3} at every observing time are used to distinguish two stages. In ECS region (Figure 1D), the points where ascent and descent cease are identified as the turning points for three stages.

2.3 Reanalysis datasets

Aerosol property is represented by the total extinction optical depth (AOD) from hourly time-averaged 2-dimensional data collection in Modern-Era Retrospective analysis for Research and Applications version 2 (MERRA-2), with a spatial resolution of 0.5° × 0.625° (Buchard et al., 2017). It is interpolated onto a 1° × 1° grid using bilinear interpolation method.

Meteorological indicators related to cloud microphysical process including sea surface temperature (SST), lower-tropospheric stability (LTS), relative humidity on 700 hPa and 1000 hPa (RH700 and RH1000), vertical velocity on 800hPa (omega800), horizontal wind field at 700 hPa and horizontal temperature advection at the surface (SST_{adv}) are either obtained or calculated by ERA5 reanalysis data (Hersbach et al., 2020). ERA5 is the fifth-generation atmospheric reanalysis of global climate and is produced using the ECMWF's Integrated Forecast System cycle 41r2 with a 4-dimension variation assimilation system. Compared to the ERA-Interim, ERA5 has higher spatial (0.25° × 0.25°) and temporal resolutions (hourly), and the representation of atmospheric processes has been further improved. ERA5 reanalysis data is matched to SatCORPS data in the same way as GPM_3IMERGHH.

LTS is expressed as the difference of potential temperature between 700 hPa and surface (Klein and Hartmann, 1993).For the horizontal temperature advection at the surface (SST_{adv}), it may be expressed in spherical coordinate as Jian et al. (2021) and Qu et al. (2015):

$$SST_{adv} = -\frac{u}{R_E \cos\phi}\frac{\partial SST}{\partial \lambda} + \frac{v}{R_E}\frac{\partial SST}{\partial \phi} \quad (2)$$

where R_E is the mean Earth radius, SST is the surface skin temperature, u and v are the eastward and northward horizontal 10 m wind components, respectively. Φ and λ represent the radians of latitude and longitude. A positive/negative SST_{adv} indicates warm/cold advection, which influences the surface latent and sensible heat fluxes then the moisture transport within the cloud

https://doi.org/10.5194/egusphere-2024-3601
Preprint. Discussion started: 16 December 2024

155 layer and the cloud thickness (George and Wood, 2010) and, consequently, influence the cloud liquid water.

3 Results

3.1 LWP adjustments vary alongside microphysical-dynamical conditions

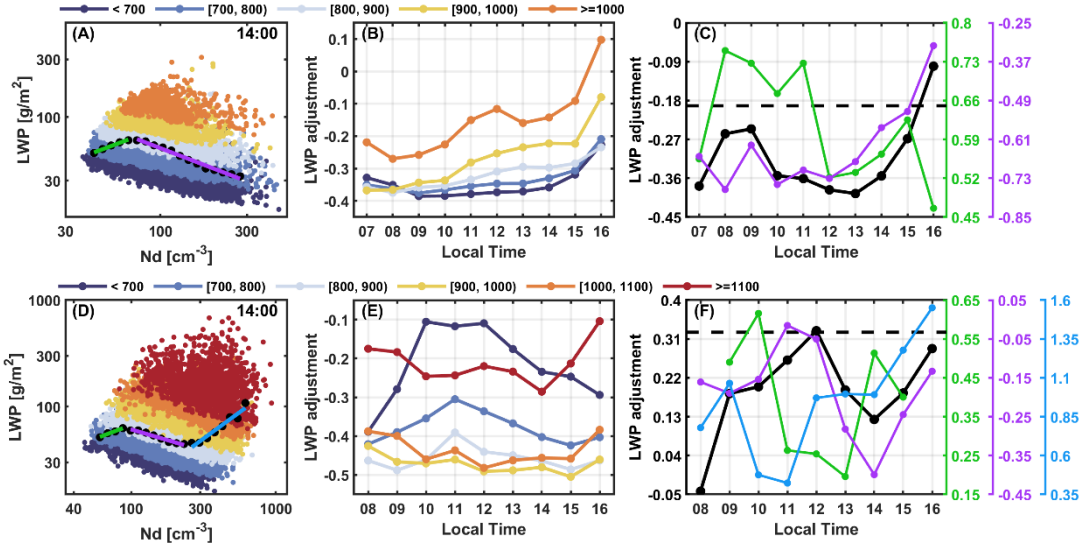

Figure 1. LWP adjustments in log-log spaces and their diurnal patterns in two typical regions (the west of Australia, 160 **AUW) and the east China sea, ECS).** Non-precipitation cloud samples scattered in N_d-LWP log space at 1400 LT in (A) AUW and (D) ECS region. Colored dots are samples in different cloud thickness (H) bins (unit: m). Black dots represent median LWP in each N_d bin. The colored lines are the fits of black dots at different stages. Diurnal variations of LWP adjustments binned by H in (B) AUW and (E) ECS region are showed. Colored lines in (C) and (F) are diurnal variations of different stages in (A) and (D), while black lines are the overall diurnal variations of LWP adjustments in two regions, 165 respectively. The incompletion of green line in (F) is because the processes are not obvious at 0800 LT and 1600 LT. Dashed lines represent the average LWP adjustments considering diurnal variations, –0.19 for AUW (C) and 0.33 for ECS (F).

Figure 1 (A and D) shows the scatter plots of N_d-LWP relationship in log-log space for AUW and ECS regions at 1400 LT (local time), respectively. The complete pictures of all available daytime periods are presented in Figure S2. N_d-LWP relationships show similar patterns during daytime in each region but opposite results in two regions, with an overall negative 170 (positive) adjustment in AUW (ECS), meaning that LWP decreases (increases) with increased N_d. For non-precipitation clouds, both positive and negative LWP adjustments have been reported (Glassmeier et al., 2021; Michibata et al., 2016; Rosenfeld et al., 2019; Toll et al., 2019), caused by different mechanisms (e.g. lifetime effect and entrainment feedbacks) (Michibata et al., 2016). In fact, conflicting LWP adjustments are ultimately subject to the dominant microphysical-dynamical mechanisms for each N_d stage. In the beginning stage of aerosol-limited clouds where cloud development is limited by the availability of CCN

https://doi.org/10.5194/egusphere-2024-3601
Preprint. Discussion started: 16 December 2024

(i.e., low N_d) (Koren et al., 2014). The increased smaller droplets delay the collision−coalescence process and enhance the condensation mass which leads to the suppression of precipitation and increase of LWP. Despite of the multiple criteria to exclude precipitation (r_e < 14 μm & GPM = 0 mm/hr), local presence of drizzle is hard to be totally eliminated given that GPM IMERG products showed large bias detecting light rain events (Li et al., 2021). As drizzle forms when r_e is 12-14 μm in a modeling study (Rosenfeld et al., 2012), here a sensitivity test is performed on this standard to see whether the initial LWP increase is significantly influenced by drizzles. Results show that the increasing LWP at low N_d still remained when r_e criterion reduced to 10 μm (Figure S3-S4, insufficient samples with lower r_e). Therefore, we believe that precipitation suppression could be the main reason why we get the positive pattern in LWP for the low N_d conditions in Figure 1 (A and D, green line).

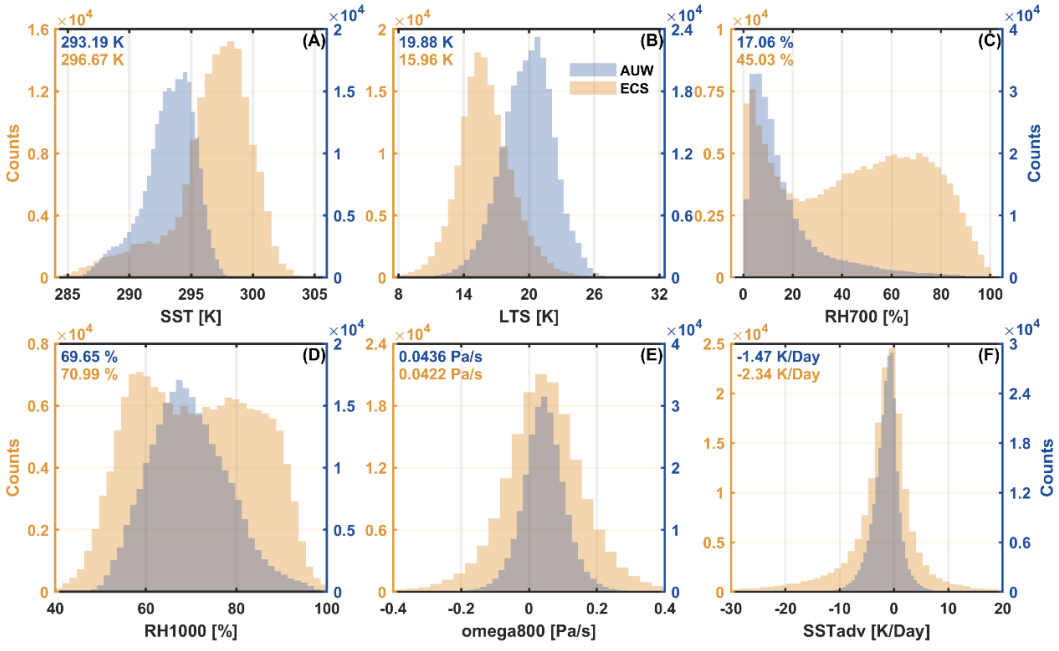

Figure 2. 4-year meteorological conditions of non-precipitation clouds in AUW and ECS region from 2016 to 2019. Histograms of meteorological factors are presented here. The mean values are labeled in the top-left corner. Data are directly or indirectly derived from ERA5. For vertical velocities on 800 hPa (omega800), positive (negative) values indicate downdraft (updraft).

As the increasing of N_d reaches a critical stage, processes at the cloud margins, such as sedimentation-entrainment feedbacks and evaporation-entrainment feedbacks (Ackerman et al., 2004; Small et al., 2009), become dominant, leading to the formation of the subsequent downward branch (purple line in Figure 1). The transition between two N_d stages corresponds to the "optimal concentration (N_{op})" concept proposed by Dagan et al. (2015). Enhanced condensation and entrainment, driven by increasing aerosols, play dominant role before and after N_{op}, respectively. ECS has a higher N_{op} than the AUW (around 76 cm^{-3} in AUW and 97 cm^{-3} in ECS), which is influenced by the respective environmental conditions of these regions. ECS is distinguished by an unstable and moist atmosphere, with a mean lower-tropospheric stability (LTS) of 15.96 K and a peak in

https://doi.org/10.5194/egusphere-2024-3601
Preprint. Discussion started: 16 December 2024

195 relative humidity on 700 hPa (RH700) of 70% (Figure 2). These moist and unstable conditions lead to clouds having a tendency to accumulate more water mass (i.e. larger N_{op}) (Dagan et al., 2015). Whereas in AUW region, over 80% of cloud samples exhibit LTS values greater than 18 K, and the RH700 above cloud top is relatively low (17% on average). The above processes result in a nonlinear pattern of N_d-LWP relationship for N_d within ~300 cm^{-3}, which is somewhat similar to the pattern of mix regime (containing both precipitation and non-precipitation samples) in previous studies (Glassmeier et al., 2021; Gryspeerdt
200 et al., 2019).

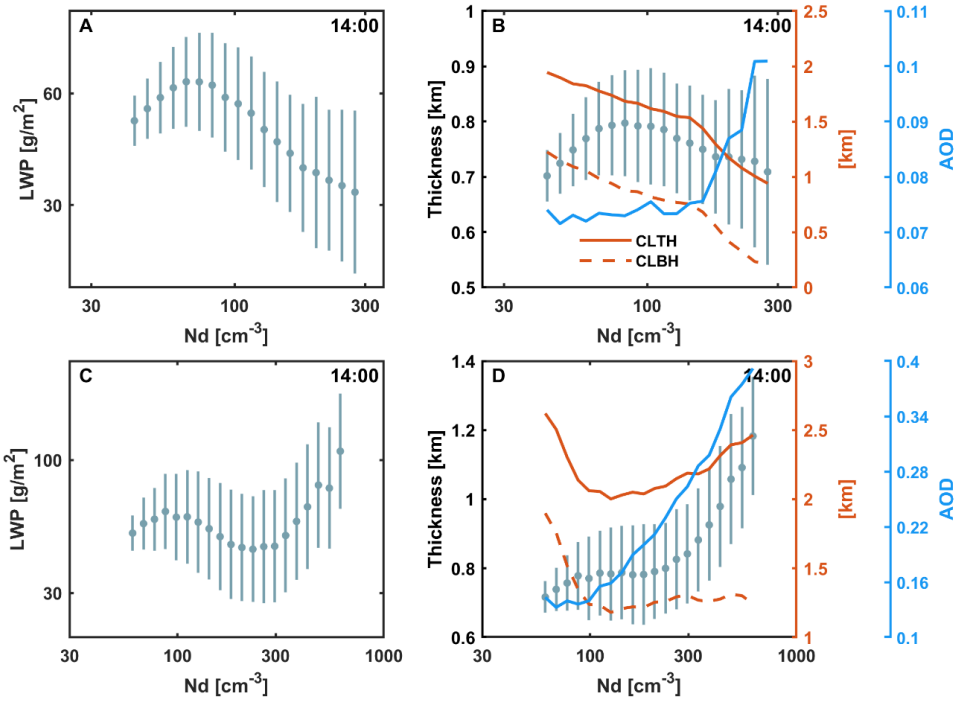

Figure 3. Comparisons between N_d-LWP relationship and N_d-Thickness relationship in two regions. Relationship between N_d and (A) LWP, (B) cloud thickness in AUW region. Relationship between N_d and (C) LWP, (D) cloud thickness in ECS region. The orange solid and dashed lines show the change of cloud top height (CLTH) and cloud bottom height (CLBH)
205 with N_d.

However, LWP begins to rise at high N_d in ECS (blue line in Figure 1D), which is the primary reason causing the overall positive LWP adjustments in this region. Positive sensitivity over ECS has been reported but not fully understood (Bender et al., 2019; Gryspeerdt et al., 2019; Michibata et al., 2016; Zhang et al., 2021). Michibata et al. (2016) attributed the positive LWP response in non-precipitation clouds over East Asia to cloud lifetime effect. Gryspeerdt et al. (2019) reported the rising
210 behavior at high N_d, especially at moist conditions, however, their samples ended around 300 cm^{-3}. Here in ECS region, clouds are heavily affected by anthropogenic aerosols, showing LWP increases with N_d at high N_d (>300 cm^{-3}). The increasing of LWP at high N_d seems to indicate the increasing N_d provides a larger surface area for condensation and finally compensating

https://doi.org/10.5194/egusphere-2024-3601
Preprint. Discussion started: 16 December 2024

the effect of entrainment (Lee et al., 2009). Furthermore, we found this behavior is consistent with deepening of cloud depth (Figure 3, C and D) which is likely induced by the latent heat released by condensation, indicating the invigoration effect by aerosols (Altaratz et al., 2014). To exclude the influence of Simpson's Paradox (thicker cloud samples along the coast with larger N_d and thinner ones with smaller N_d offshore), we divide the samples into coastal and offshore groups and found that the observed pattern is not significantly affected by the geographical region (Figure S5).

Although the microphysical-dynamical processes are challenging to be observed directly, environmental conditions can be considered as proxy and provide further support for invigoration effect. Cloud droplets are more likely to grow in the unstable and moist atmosphere in ECS. Additionally, according to the division from Rosenfeld et al. (2019), we categorize the clouds into Sc (LTS > 18 K), Sc to Cu transition (14 K ≤ LTS ≤ 18 K) and Cu (LTS < 14 K) (Figure 4, G, H and I). Clouds in ECS region are dominated by the Sc to Cu transition regime.

The formation of this transition regime is associated with increasing sea surface temperature (SST) due to "deepening-warming decoupling" (Albrecht et al., 1995; Bretherton and Wyant, 1997). Sc presents over the relatively shallow and stable boundary layer with cooler sea surface along the coast (Figure 4, A and B) and most of Sc may be mainly advected from the southeast Chinese plain (Klein and Hartmann, 1993). According to the cloud advection scheme by Miller et al. (2018), cloud advection can be approximated as the translation of the cloud field with the wind field. The advection height assumed to correspond to the height of the cloud top. Therefore, we can simply deduce from the wind field at 700 hPa that clouds in ECS have the possibility of advection from the Chinese plain in the west (Figure S6). As air moves offshore, MBL deepens and cloud layer decouples with the surface mixed layer over warmer sea surface. Cu forms in the moist and unstable subcloud layer and rises to upper cloud layer, resulting in a local cumulus-coupled MBL. Warm invigoration, in which aerosols promote water vapor condensation by acting as CCN, releasing latent heat and promoting cloud vertical development, mainly occurs in these convective clouds, consistent with Zhang et al. (2021). They also attributed the positive LWP adjustments in ECS to warm invigoration with the low-level convective clouds (Sc and Cu) domain by MODIS and CloudSat measurements. Kaufman et al. (2005) also reported larger LWP in higher aerosol loading conditions over Atlantic in warm clouds (a mix of stratus and trade cumulus). In contrast to the model results of Koren et al. (2014), who suggested that warm invigoration saturates at higher aerosol loading (AOD ~ 0.3), our findings indicate a higher AOD of 0.4 (Figure 3), which is reasonable because the saturation value of AOD exhibits regional variability. For example, Kaufman et al. (2005) reported a maximum AOD of 0.46, while Zhang et al. (2021) found that the AOD in the ECS region is approximately 0.4. Considering the different processes associated with cloud regimes, we conducted the similar analysis for each cloud regime. Our findings reveal that the pattern of LWP adjustments is insensitive to cloud regime (Figure S7-S9), suggesting that they can be studied collectively.

Additionally, the observed LWP adjustments are results of meteorological covariations (Chen et al., 2014; Engström and Ekman, 2010; Zhang and Feingold, 2023). When we discuss ACI, the intricate interplay among meteorological factors, clouds and aerosols makes it difficult to exclude the influences from meteorological factors. Previous studies have employed various methods to exclude environmental confounding factors, such as opportunistic experiments from ship-track or volcano eruptions (Chen et al., 2022; Toll et al., 2019) where an overall weak LWP adjustment is observed. For satellite studies,

https://doi.org/10.5194/egusphere-2024-3601
Preprint. Discussion started: 16 December 2024

Rosenfeld et al. (2019) pointed out that cloud thickness (H) explained almost three-fourths of meteorological impacts on cloud radiative effect (CRE) and they demonstrated an overall positive LWP adjustments when separating H. However, applying their method and constraining H in all intervals of Figure 1 (B and E), we find that LWP adjustments become negative, indicating that entrainment processes dominate LWP adjustments. The discrepancy may arise from their focus on samples in convective cores (top 10% of cloud optical thickness), which are closer to adiabatic, whereas our samples suggest more exchange with the free atmosphere.

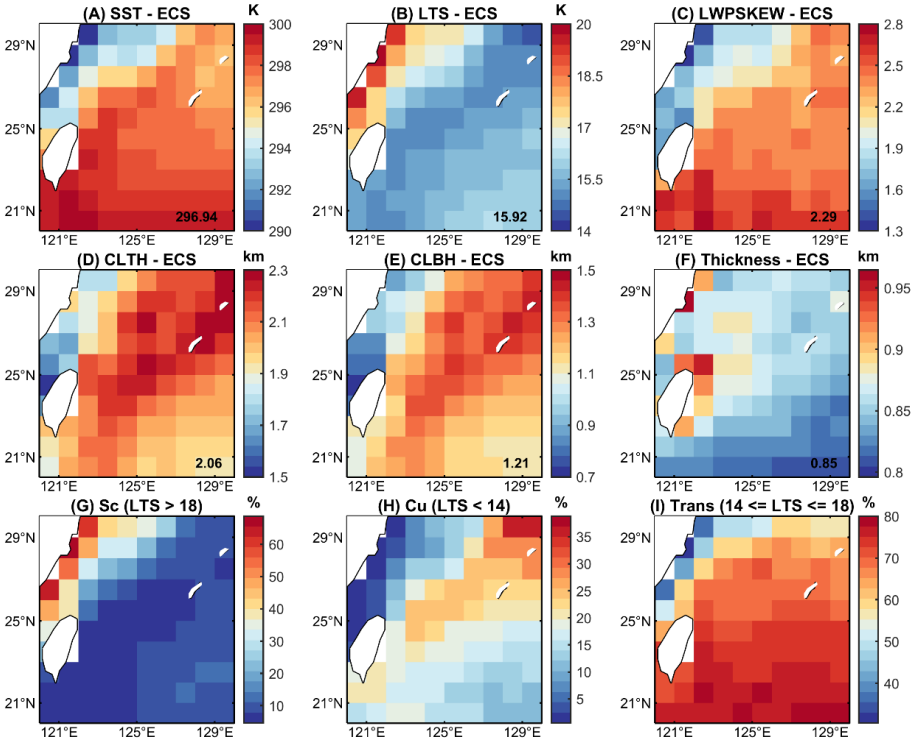

Figure 4. Distributions of meteorological factors and different cloud regimes in ECS region. (A) Sea Surface Temperature (SST) and (B) lower-tropospheric stability (LTS) are from ERA5 reanalysis data. (C) LWP skewness, (D) cloud-top height (CLTH), (E) cloud bottom height (CLBH) and (F) cloud thickness are directly or indirectly derived from SatCORPS Himawari-8 product. The numbers in the lower right corner represent regional averages being weighted by the cosine of latitude. Distribution of the proportion of cloud regimes for (G) Stratocumulus (Sc, LTS > 18 K), (H) Cumulus (Cu, LTS < 14 K), (I) Sc to Cu transition regime (Trans, 14 K <= LTS <= 18 K).

Fons et al. (2023) suggested H is an important confounder using causal approach and should be conditioned on. Here our results indicate the physical significance of constraining H. The sensitivity of LWP adjustments to H is clearly observed in Figure 1. In AUW region, negative LWP adjustments become weaker as H increases. This indicates that clouds of different H respond differently to entrainment. Thicker clouds with larger r_e are less sensitive to entrainment-feedback with increasing N_d compared to thinner clouds (Figure 1A). In other words, LWP in different H intervals responds differently to N_d so it is

https://doi.org/10.5194/egusphere-2024-3601
Preprint. Discussion started: 16 December 2024

necessary to restrict H in order to exclude the effects of covariation. However, in ECS region, negative LWP adjustments for clouds with H < 900 m become stronger with increasing H, while for clouds with H > 900 m, quite the contrary: it weakens with increasing H. The bidirectional sensitivity of LWP adjustments to H is likely attributed to distinct mixing characteristics among different cloud regimes in ECS region, reflecting the complex interactions between meteorological factors, clouds, and aerosols. Additionally, clouds above 800m are associated with warm invigoration process (Figure 3). In this condition, H serves as a mediator but not a confounder. This implies that constraints on H in ECS is inappropriate because it fundamentally restricts a majority of mechanisms influencing cloud vertical development.

In summary, the above results reveal that LWP adjustments strongly depend on microphysical-dynamical processes (e.g. precipitation suppression, entrainment feedbacks and warm invigoration) and meteorological conditions (e.g. moisture and stability of the boundary layer). Given that some of these factors display diurnal variations in response to the solar radiation cycle, LWP adjustments would also exhibit diurnal patterns (black lines in Figure 1, C and F). We surmise that the prevailing dynamic conditions at any given time are responsible for the observed diurnal variations of LWP adjustments. To verify this hypothesis, we investigated the diurnal variations in LWP adjustments and their potential influencing factors.

3.2 How LWP adjustments change over diurnal scale and mechanisms

In AUW region, the negative LWP adjustments strengthen from around 0900 LT to 1300 LT, reaching the strongest at –0.38, and then weaken to –0.10. In ECS region, the positive LWP adjustments exhibit two local peaks during the observation period, occurring at 1200 LT and 1600 LT, with peak values of 0.33 and 0.29, respectively. Additionally, two local minima LWP adjustments are observed at 0800 LT and 1400 LT, with values of –0.04 and 0.12, respectively (Figure 1, C and F). The cloud-topped marine boundary layer (MBL) has been demonstrated to exhibit strong diurnal changes (Duynkerke and Hignett, 1993). Due to the observational limitations with passive satellite, it is not feasible to study the variations of MBL directly through its vertical profiles as with in-situ observations or active satellite (Albrecht et al., 1995; Luo et al., 2016). Instead, we can indirectly infer the boundary layer processes by examining the diurnal variations of cloud properties.

AUW is one of the subtropical Sc regions over the eastern part of the ocean away from continent (Klein and Hartmann, 1993), characterized by large LTS and strong large-scale subsidence (Figure 2), which are conditions favorable for the formation of Sc. Figure 5 depicts the diurnal variations of cloud properties in the Sc-like AUW region. The diurnal variation of LWP shows a typical pattern with a peak in the morning and a gradual reduction until early afternoon. This pattern of variation is subject to diurnal cycle of solar insolation (Bretherton et al., 2004; Mechoso et al., 2014; Wood et al., 2002). Specifically, during daytime, solar radiation absorption within the cloud layer and long-wave cooling at cloud top drive the turbulent mixing within the cloud layer and inhibit turbulence to the sea surface, thus leading to the decoupling of MBL (Duynkerke and Hignett, 1993; Ghosh et al., 2005; Slingo et al., 1982). As decoupling cuts off the moisture source from the sea surface, the imbalance between entrainment drying and upward moisture flux may thin the cloud layer. The decrease of LWP before 1300 LT is primarily attributed to the lifting of cloud base which is in line with early modeling study for typical Sc cloud regimes (Bougeault, 1985), indicating that entrainment drying originates from evaporation at cloud base. After 1300

https://doi.org/10.5194/egusphere-2024-3601
Preprint. Discussion started: 16 December 2024

LT, LWP no longer decreases and even slightly increases. This is because the gradual reduction of solar heating after 1300 LT hinders the intensification of decoupling and helps rebuild the turbulence between the cloud and subcloud layer. Therefore, LWP remains nearly constant after 1300 LT likely due to the balance between entrainment drying and the reconstruction of turbulence.

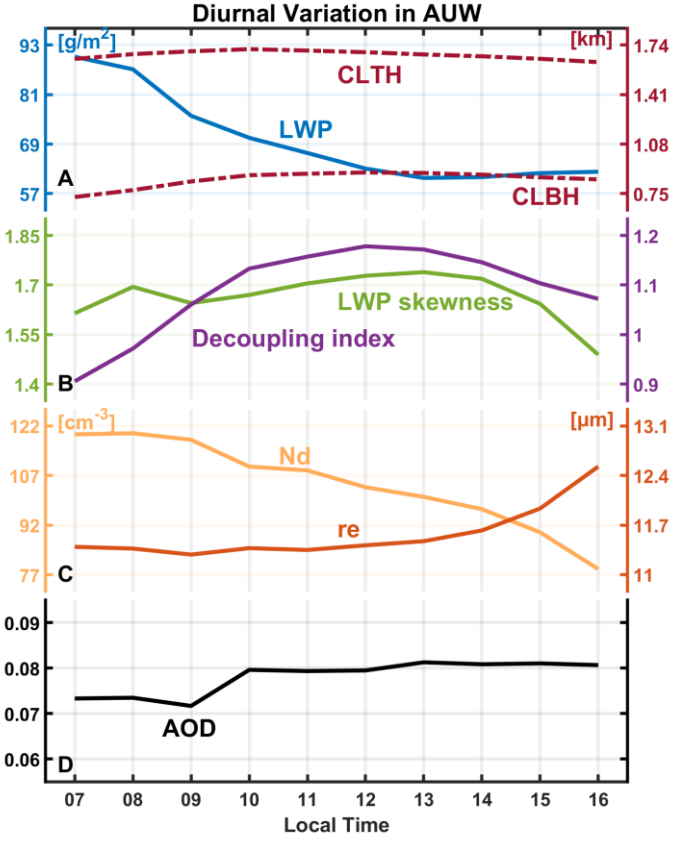

Figure 5. Diurnal patterns in AUW region. (A) Cloud liquid water path (LWP), cloud-top height (CLTH) and cloud bottom height (CLBH). (B) LWP skewness and decoupling index in AUW region. (C) Cloud droplet number concentration (N_d) and effective radius (r_e). (D) Aerosol optical depth (AOD).

Following the quantification method of Zheng et al. (2018) and Kazil et al. (2017), this study presents auxiliary verifications of decoupling process. First, according to Zheng et al. (2018), decoupling of the subtropical Sc decks during cold advection is often unstable (negative temperature advection). The formation of Cu beneath the Sc will render local coupling through feeding moisture into the upper cloud layer thus causing a positive skewness of probability density function (PDF) of LWP. Therefore, the skewness of LWP PDF can be used to estimate the degree of decoupling for each cloud sample:

$$\text{skewness} = \frac{\mathrm{E}(\mathrm{x}-\mathrm{u})^3}{\sigma^3} \quad (3)$$

where E is the expected value, μ and σ is the mean standard deviation of x, respectively. Positive skewness indicates more data

https://doi.org/10.5194/egusphere-2024-3601
Preprint. Discussion started: 16 December 2024

tends to be distributed to the right, vice versa.

As shown in Figure 5, LWP skewness increases before 1300 LT and then decreases, illustrating the decoupling process and turbulence reconstruction discussed above. Note that while the cumulus penetration alters LWP, small variations in LWP skewness suggest that it cannot be directly compared with the reduction of LWP caused by decoupling, thus having no evident effect on the diurnal variation of LWP over AUW region. Additionally, another decoupling index defined by Kazil et al. (2017) shows similar variation with LWP skewness, quantifying the relative position between the CLBH and the lifting condensation level (LCL). A larger index implies a stronger degree of decoupling:

$$\text{decoupling index} = \frac{CLBH - LCL}{LCL} \tag{4}$$

The two indexes support each other and confirm the decoupling process.

Unexpectedly, there is no evident diurnal variation of AOD in AUW, but N_d continually declines from 0700 LT to 1600 LT and re does not change significantly before 1200 LT and then rises. It is thus reasonable to infer the diurnal variations of N_d and r_e are related with dynamic process on account of the disagreement with aerosols variations. Before 1200 LT, the decoupling that cuts off moisture transport suppresses condensational growth, while the shortwave heating counteracts longwave cooling, resulting in weakening of cloud-top entrainment (Verlinden, 2018.). The combination of these two processes leads to the little variation in r_e. Additionally, the continuous decrease in N_d before 1300 LT may be attributed to the suppression of both surface moisture transport and cloud base updrafts (Stevens, 2000), which in turn reduce the supersaturation and hence the number of activated cloud droplets (Twomey, 1959). After 1200 LT, CLTH begins to decrease, according to $\frac{dCLTH}{dt} = w_s + w_e$ (Painemal et al., 2013), suggesting an intensification of large-scale subsidence (w_s, always negative in Sc region) and/or a weakening of entrainment rate (w_e). As large-scale subsidence becomes stronger, enhancing the temperature-inversion jump, which will in turn decrease the entrainment rate (Painemal et al., 2013). During this period, the condensational growth by the reconstructed water vapor supply will enhance re. Meanwhile, the coalescence process, enhanced by an increase in r_e leads to a decrease in N_d. This process could be more dominant than the increase in activated cloud droplets caused by water vapor reestablishment for an increase in N_d to be observed in this study.

Based on the diurnal mechanisms of MBL discussed above, the diurnal pattern of LWP adjustments is primarily a consequence of the influence of these diurnal-related mechanisms on the relationship between N_d and LWP across different microphysical-dynamical conditions. In AUW, the variation of the overall LWP adjustments (black line in Figure 1C) before 1300 LT is mainly attributed to the gradual thinning of clouds, which reduces water achievable for rain suppression under aerosol-limited state (green line). After 1300 LT, the variation in LWP adjustments is mainly governed by changes in the entrainment process (purple line). During this time, cloud-top entrainment weakens, as discussed earlier, leading to a reduction in the negative LWP adjustments over AUW region. As mentioned in the last section, the overall LWP adjustments are results of the covariance of clouds with varying thicknesses. When constrained by H, our analysis reveals that the diurnal variations of LWP adjustments align with the weakening of the cloud entrainment process. Throughout the day, this weakening is more pronounced in thicker clouds, particularly before 1200 LT, where the effects are especially significant. The reduction in

https://doi.org/10.5194/egusphere-2024-3601
Preprint. Discussion started: 16 December 2024

entrainment during this period is primarily attributed to shortwave heating. Since shortwave heating has a greater impact on thicker clouds (Petters et al., 2012), we observe a more substantial weakening in the LWP adjustments of these clouds.

In contrast, conditions of MBL in ECS region are more complicated. As mentioned in last section, ECS is a transition region due to "deepening-warming" process. Under this condition, MBL is never fully coupled but exhibits local cumulus coupling. Apparently, LWP skewness is a more appropriate indicator to reflect cumulus coupling in this region. Furthermore, the spatial distribution of LWP skewness can indicate the influence of cumulus coupling offshore (Figure 4C). For diurnal variations in ECS in Figure 6, there is a general decrease of LWP before 1300 LT followed by an increase. This is contrast to the pronounced cloud thinning observed in the AUW region due to the decoupling of MBL by solar heating. In the ECS region, the overall change of LWP is not significant (less than 10 g/m^2). Since MBL is never fully coupled, these minor observed changes are mainly caused by local cumulus coupling. The variations of LWP and LWP skewness exhibit a strong consistency. We also calculate the coefficient of variation (c_v) of CLOT to represent the uniformity of each cloud sample. c_v is defined as the standard deviation (σ) divided by the mean(μ):

$$c_v = \frac{\sigma}{\mu} \tag{5}$$

The smaller the c_v is, the less dispersion there is among the cloud pixels in the cloud sample, resulting in a more uniform sample. It turns out that the cloud layer is influenced primarily by the strength of cumulus coupling, rather than other factors.

Diurnal variations of cumulus coupling can be also attributed to solar insolation. In the Sc to Cu transition region, the decoupled cloud layer and subcloud layer are often separated by a stable transition layer, which has been widely observed by the Atlantic Stratocumulus Transition Experiment (ASTEX) conducted over the northeast Atlantic Ocean. Based on ASTEX, Roger et al. (Rogers et al., 1995) suggested that the shortwave radiation would hinder convection during daytime by increasing the stability of the transition layer. Miller et al. (1998) extended this theory to the diurnal variations and believed that the diurnal variation of Cu development was regulated by the stability of the transition layer. Applying the theory to this area, the strongest stability of the transition layer occurs at 1300 LT due to absorption of solar radiation, at which point cumulus activity is the weakest. The earlier occurrence of the strongest stability in this study compared to the observations made during ASTEX may be attributed to the environment in the ECS region, which is more favorable for cumulus convection formation. This suggests that spontaneous convection is more likely to penetrate the transition layer in the ECS region.

In terms of microphysical properties, N_d in ECS decreases before 1100 LT and then increases. Variations of r_e are just the opposite except insignificant change since 1400 LT. The crucial mechanism leading to such changes may be attributed to the weakest entrainment drying at 1100 LT, resulting in the highest values of r_e and lowest values of N_d. And the change before 1100 LT may include the impacts of reducing AOD. Additionally, subsidence from both cloud top and bottom occurred after 1400 LT limits the entrainment and the continuous decline of r_e. But N_d continues to increase due to the effect of cumulus coupling after 1400 LT (Martin et al., 1995). Such diurnal variations in entrainment have also been observed in other coastal areas. Caldwell et al. (2005) reported the weakest entrainment rate at 1100 LT during East Pacific Investigation of Climate (EPIC) stratocumulus cruise in 2001. Painemal et al. (2017) found the minimum of entrainment occurred between 0900-1100

https://doi.org/10.5194/egusphere-2024-3601
Preprint. Discussion started: 16 December 2024

LT over the northeast Pacific region, attributing the diurnal pattern to the turbulence caused by long-wave radiative cooling.

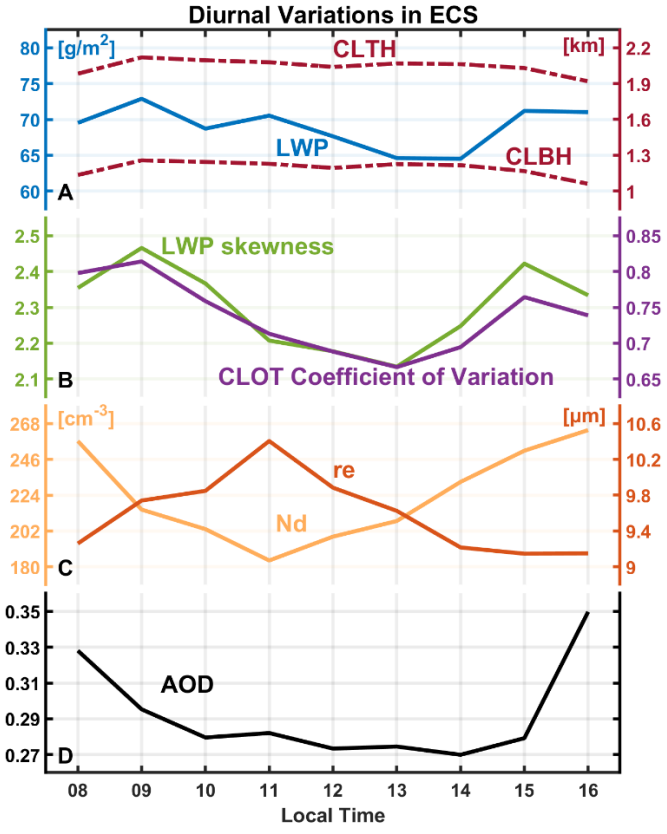

Figure 6. Diurnal patterns in ECS region. (A) Cloud liquid water path (LWP), cloud-top height (CLTH) and cloud bottom height (CLBH). (B) LWP skewness and coefficient of variation (c_v) of cloud optical depth (CLOT) in AUW region. (C) Cloud droplet number concentration (N_d) and effective radius (r_e). (D) Aerosol optical depth (AOD).

The diurnal variation of LWP adjustments in ECS is closely related to the diurnal changes in entrainment (black line in Figure 1F). As illustrated above, LWP adjustment controlled by entrainment is the weakest at 1100 LT as expected and strongest at 1400 LT (purple line). The subsequent weakening observed after 1400 LT is possibly attributed to cloud-top subsidence. It is noteworthy that the intensities of the blue line (positive) and the purple line (negative) vary consistently, but after 1400 LT, their intensities diverge. The diurnal variation of LWP adjustments controlled by warm invigoration is consistent with cumulus activities (green line) with the lowest value at 1300 LT, yet it exerts little impact on the overall diurnal variation of LWP adjustments.

Finally, Figure 7 depicts schematics of the dominant mechanisms in the two regions. In AUW region, the primary mechanism behind diurnal variation of LWP adjustments is the cloud thinning driven by MBL decoupling before 1300 LT. After 1300 LT, the gradual weakening of cloud-top entrainment mitigates the negative LWP adjustments. In ECS region, however, the H correlates with the intensity of cumulus coupling, while diurnal changes in entrainment dictate the diurnal

https://doi.org/10.5194/egusphere-2024-3601
Preprint. Discussion started: 16 December 2024

395 variation of LWP adjustments. To summarize, the diurnal variations of LWP adjustments are primarily regulated by boundary layer dynamic processes. Failure to accurately capture these diurnal variations in LWP adjustments and the underlying physical processes in observational studies may result in substantial inaccuracies in the quantification of regional and global LWP adjustments.

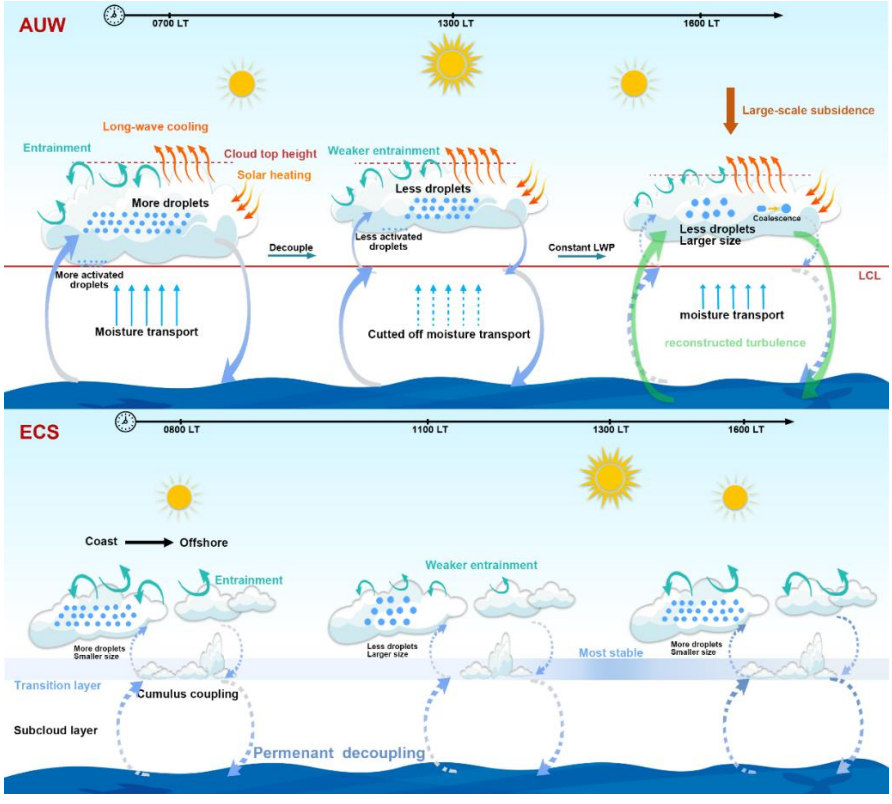

400 **Figure 7. Schematics of diurnal dominant mechanisms observed in AUW and ECS regions. See text for details.** Only the primary mechanisms are presented, while the relatively unimportant ones are omitted. Note that we represent the lifting condensation level (LCL) and transition layer at the same altitude for intuition. However, this depiction does not imply that their heights remain constant throughout the diurnal variation.

3.3 Impacts on aerosol indirect radiative effect if neglecting diurnal variations

405 Regional geostationary satellites observation reveals the significant impact of regional diurnal dynamic processes on LWP adjustments. LWP adjustments vary from –0.38 to –0.10 in AUW and from –0.04 to 0.33 in ECS. Diurnal averaged LWP adjustments are –0.19 and 0.33 considering the diurnal processes, respectively. The averaged LWP adjustment (dashed line in Figure 1, C and F) is not a simple average of the values, rather, it is derived from all available data within the region, accounting for diurnal covariation. This implies the inadequacy of previous observations only based on polar-orbiting satellites.
410 For example, for Sc in AUW region, if LWP adjustments observed by polar-orbiting satellite (such as MODIS overpass for

https://doi.org/10.5194/egusphere-2024-3601
Preprint. Discussion started: 16 December 2024

aqua at 1330 LT or terra at 1030 LT) are applied to represent the whole day, the negative LWP adjustments will be obviously overestimated because the polar-orbiting observations failed to capture the weaker entrainment process in the late afternoon. This bias will ultimately affect our estimation of cloud brightening in Twomey effect. The cloud albedo (A_c) susceptibility to aerosols can be estimated as Bellouin et al. (2020):

$$S = \frac{dA_C}{dN_d} = \frac{A_C(1 - A_C)}{3N_d}\left(1 + \frac{5}{2}\frac{d\ln LWP}{d\ln N_d}\right) \quad (6)$$

where S is the sensitivity of cloud albedo. According to this equation, LWP adjustments serve to regulate the cooling effect of the Twomey effect (the first term).

Following the method of (Glassmeier et al., 2021), we assume that climatological A_c is approximated as a constant value of the steady-state. Then the impact of LWP adjustments on S depends on $\left(1 + \frac{5}{2}\frac{d\ln LWP}{d\ln N_d}\right)$ according to Eq. 6. If we only consider LWP adjustments at fixed moments but neglect the diurnal variations, the cooling effect of LWP adjustments (strengthen Twomey effect) will be severely underestimated. For example, the average LWP adjustments at MODIS Aqua and Terra overpasses (1030 LT and 1330 LT) are −0.37 in AUW region and 0.20 in ECS region, respectively. The daily average LWP adjustments for the two regions are −0.19 and 0.33, respectively. After substituting these values into $\left(1 + \frac{5}{2}\frac{d\ln LWP}{d\ln N_d}\right)$, the cooling effect of LWP adjustments will be underestimated by |(0.525−0.075)/0.525|×100% = 86% in AUW region if neglecting the diurnal variations. This bias will lead to a further |(-0.37-(-0.19))/(−0.4)|×100% = 45% offset of the Twomey effect, as the Twomey effect is completely offset when the LWP adjustment is −0.4. Thereby the offset will steer aerosol indirect radiative effect towards a warming direction. Similarly, these two estimates are 18% and 30% for ECS region.

4 Discussion

Our analysis reveals the diurnal variations of LWP adjustments in two specific regions within the sight of Himawari-8, along with the possible mechanisms contributing to these variations. The observational studies demonstrate LWP adjustments in two regions are determined by the dominant microphysical-dynamical processes in different N_d stages, while their diurnal variations depend on dynamical conditions of boundary layer. In AUW region, diurnal variations are primarily associated with the decoupling process of MBL and cloud-top entrainment, while in ECS region they are predominantly governed by the diurnal changes in cloud-top entrainment processes. Our findings in the AUW region align closely with the large eddy simulation (LES) studies of stratocumulus clouds conducted by Zhang et al. (2024), who attributed the diurnal pattern to a buffering effect induced by shortwave heating. In contrast, we focus on discussing the dynamical mechanisms to the given environment. Additionally, we identified different diurnal pattern and dominant mechanisms in ECS region. LWP adjustments contribute to a broad range of uncertainties in the effective radiative forcing of ACI (ERF_{aci}) (IPCC, 2023). Here, we emphasize the time-dependent uncertainty observed by geostationary satellites, primarily stemming from varying dominant mechanisms at different times throughout the day. This is essentially a meteorological covariation on the daily time scale. We indicate an

https://doi.org/10.5194/egusphere-2024-3601
Preprint. Discussion started: 16 December 2024

overall underestimation of cooling effect up to 86%, with a further 45% offset of the Twomey effect when neglecting the diurnal variations of LWP adjustments. Furthermore, our results quantify the impact of boundary layer feedback on LWP adjustments. For example, diurnal variations of cloud-top entrainment in ECS region result in a 112% variation of LWP adjustments within the daytime relative to the daily mean (the diurnal variation range divided by daily mean), assuming other conditions remain relatively unchanged.

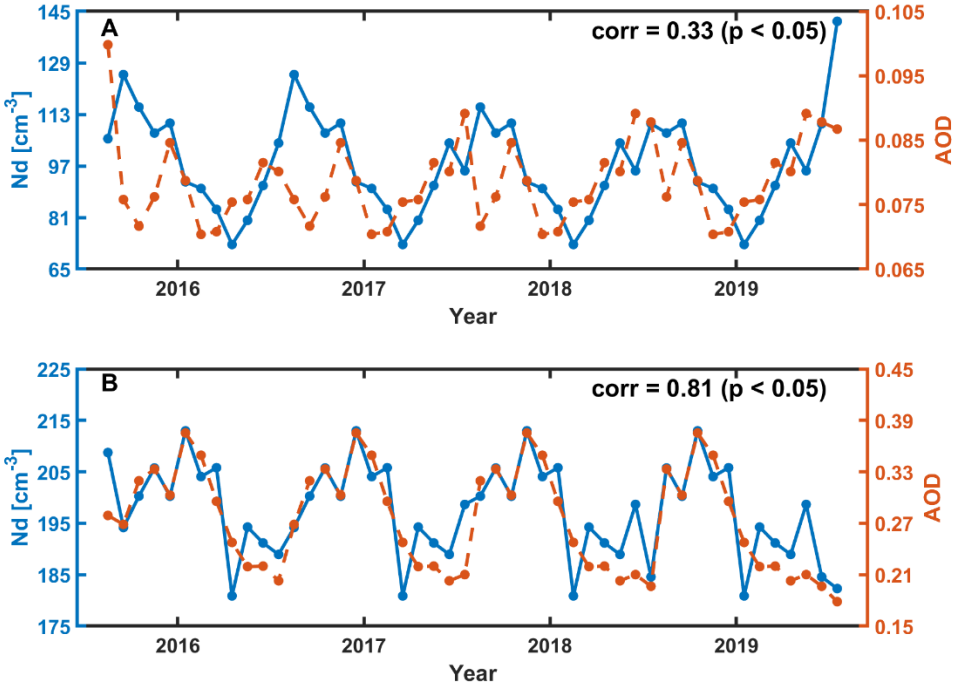

Figure 8. 4-year long-term variations of N_d and aerosol optical depth (AOD) from MERRA-2 at 1200 LT in AUW (A) and ECS (B) region. The correlation coefficients (corr) between N_d and AOD are 0.33 and 0.81 (significant at the 95% confidence level), respectively.

It is worth noting that our results also reveal diurnal variations of N_d, a core indicator in ACI, which are also attributed to the MBL diurnal processes. While previous studies have analyzed the long-term variations of N_d, highlighting the key role of aerosols (Hu et al., 2021; Li et al., 2018; McCoy et al., 2015, 2018; Quaas et al., 2006), unexpectedly, there is no good consistency between them in diurnal variations. This discrepancy may stem from previous polar-orbiting satellite observations at fixed times have overlooked the crucial role played by other physical mechanisms at different times. In fact, geostationary satellite assessments (Figure 8) uncover significant correlations observed between the 4-year long-term variations of AOD and N_d at 1200 LT in both regions, particularly in ECS with a correlation of 0.81. Meanwhile, both regions show the similar distribution patterns, with higher N_d and smaller r_e near the continental coastal area, aligning with the average AOD spatial distribution (spatial correlation coefficients of 0.84 in AUW and 0.91 in ECS) (Figure S1), suggesting a pronounced impact of

https://doi.org/10.5194/egusphere-2024-3601
Preprint. Discussion started: 16 December 2024

anthropogenic activities on cloud microphysical properties on a long-term scale. Note that the correlations between AOD and N_d at certain fixed times are not statistically significant (not shown). This may be due to the relatively insignificant impact of aerosol effects at these moments, while other physical processes may exert a more pronounced influence. Future researches should broaden its scope to investigate effects of other physical processes on N_d at specific times, in addition to the roles of aerosols. Moreover, in the context of global warming, whether these physical processes will be affected and consequently contribute to variations of N_d deserves further investigation.

Several limitations should be acknowledged in this study. First, the time-dependence of LWP adjustments we discussed differs from the cloud evolution process, emphasizing diurnal variations caused by changes in dominant mechanisms at different times rather than tracking the evolution of individual clouds. This approach may introduce uncertainties into our results since the full cloud life cycle and evolution is not the same with diurnal variations. The full cloud lifetime evolution associated with LWP adjustments is not the scope of this study and warrant further exploration. Additionally, given the scarcity of observational data at fine scales, certain mechanisms are indirectly inferred from observational index (e.g., decoupling process inferred from LWP skewness), which needs further microphysical-process based in-situ observations as well as model simulations. Finally, uncertainties of retrievals have been discussed in Data and Methods, which provides further context for the limitations of our study.

In summary, our research provides a novel perspective for investigating the diurnal variation of LWP adjustments, focusing on how microphysical-dynamical processes in clouds are influenced by the diurnal variations of the boundary layer processes. We underscore the importance of fully considering the covariation with environmental conditions, indicating different potential influencing factors on cloud brightening and radiative forcing in terms of the regional and diurnal daytime scale.

Data availability

The datasets that support this study are all available to public. The SatCORPS Himawari-8 product is available at https://asdc.larc.nasa.gov/project/CERES. The MERRA-2 product is available at https://disc.gsfc.nasa.gov/datasets/M2T1NXAER_5.12.4/summary?keywords=merra2. The GPM_3IMERGHHV07 is available at https://disc.gsfc.nasa.gov/datasets/GPM_3IMERGHH_07/summary?keywords=gpm%20imerg. ERA5 reanalysis data is available at https://cds.climate.copernicus.eu/. All data are available in the main text or the supporting information.

Author contributions

JiaL and YaW performed the analysis and organized the original manuscript. JimL and YaW conceptualized the study and reviewed the manuscript. WZ assisted in data analysis and validation. LZ and YuW assisted in investigation and the final review and editing of the manuscript.

https://doi.org/10.5194/egusphere-2024-3601
Preprint. Discussion started: 16 December 2024

Competing interests

The contact author has declared that noneof the authors has any competing interests

Acknowledgements

We would like to acknowledge ChatGPT for its role in polishing the language for the text. We would like to acknowledge freepik.com for supporting icons used in our schematics (www.freepik.com).

Financial support

This work is supported by the following funding: Key Program of the National Natural Science Foundation of China (42430601), Major Program of the National Natural Science Foundation of China (42090030), National Natural Science Foundation of China (42175087), Science and Technology Project of Gansu Province (Outstanding Youth Fund, 24JRRA386).

References

Ackerman, A. S., Kirkpatrick, M. P., Stevens, D. E., and Toon, O. B.: The impact of humidity above stratiform clouds on indirect aerosol climate forcing, Nature, 432, 1014–1017, https://doi.org/10.1038/nature03174, 2004.

Albrecht, B. A.: Aerosols, Cloud Microphysics, and Fractional Cloudiness, Science, 245, 1227–1230, https://doi.org/10.1126/science.245.4923.1227, 1989.

Albrecht, B. A., Bretherton, C. S., Johnson, D., Scubert, W. H., and Frisch, A. S.: The Atlantic Stratocumulus Transition Experiment—ASTEX, Bulletin of the American Meteorological Society, 76, 889–904, https://doi.org/10.1175/1520-0477(1995)076<0889:TASTE>2.0.CO;2, 1995.

Altaratz, O., Koren, I., Remer, L. A., and Hirsch, E.: Review: Cloud invigoration by aerosols—Coupling between microphysics and dynamics, Atmospheric Research, 140–141, 38–60, https://doi.org/10.1016/j.atmosres.2014.01.009, 2014.

Bellouin, N., Quaas, J., Gryspeerdt, E., Kinne, S., Stier, P., Watson-Parris, D., Boucher, O., Carslaw, K. S., Christensen, M., Daniau, A. -L., Dufresne, J. -L., Feingold, G., Fiedler, S., Forster, P., Gettelman, A., Haywood, J. M., Lohmann, U., Malavelle, F., Mauritsen, T., McCoy, D. T., Myhre, G., Mülmenstädt, J., Neubauer, D., Possner, A., Rugenstein, M., Sato, Y., Schulz, M., Schwartz, S. E., Sourdeval, O., Storelvmo, T., Toll, V., Winker, D., and Stevens, B.: Bounding Global Aerosol Radiative Forcing of Climate Change, Rev. Geophys., 58, https://doi.org/10.1029/2019RG000660, 2020.

Bender, F. A.-M., Frey, L., McCoy, D. T., Grosvenor, D. P., and Mohrmann, J. K.: Assessment of aerosol–cloud–radiation correlations in satellite observations, climate models and reanalysis, Clim Dyn, 52, 4371–4392, https://doi.org/10.1007/s00382-018-4384-z, 2019.

Bennartz, R.: Global assessment of marine boundary layer cloud droplet number concentration from satellite, J. Geophys. Res.,

https://doi.org/10.5194/egusphere-2024-3601
Preprint. Discussion started: 16 December 2024

112, D02201, https://doi.org/10.1029/2006JD007547, 2007.

Bennartz, R. and Rausch, J.: Global and regional estimates of warm cloud droplet number concentration based on 13 years of AQUA-MODIS observations, Atmos. Chem. Phys., 17, 9815–9836, https://doi.org/10.5194/acp-17-9815-2017, 2017.

Boers, R., Acarreta, J. R., and Gras, J. L.: Satellite monitoring of the first indirect aerosol effect: Retrieval of the droplet concentration of water clouds, Journal of Geophysical Research: Atmospheres, 111, https://doi.org/10.1029/2005JD006838, 2006.

Bougeault, P.: The Diurnal Cycle of the Marine Stratocumulus Layer: A Higher-Order Model Study, Journal of the Atmospheric Sciences, 42, 2826–2843, https://doi.org/10.1175/1520-0469(1985)042<2826:TDCOTM>2.0.CO;2, 1985.

Brenguier, J.-L., Burnet, F., and Geoffroy, O.: Cloud optical thickness and liquid water path – does the *k* coefficient vary with droplet concentration?, Atmospheric Chemistry and Physics, 11, 9771–9786, https://doi.org/10.5194/acp-11-9771-2011, 2011.

Bretherton, C. S. and Wyant, M. C.: Moisture Transport, Lower-Tropospheric Stability, and Decoupling of Cloud-Topped Boundary Layers, Journal of the Atmospheric Sciences, 54, 148–167, https://doi.org/10.1175/1520-0469(1997)054<0148:MTLTSA>2.0.CO;2, 1997.

Bretherton, C. S., Uttal, T., Fairall, C. W., Yuter, S. E., Weller, R. A., Baumgardner, D., Comstock, K., Wood, R., and Raga, G. B.: The Epic 2001 Stratocumulus Study, Bulletin of the American Meteorological Society, 85, 967–978, https://doi.org/10.1175/BAMS-85-7-967, 2004.

Bretherton, C. S., Blossey, P. N., and Uchida, J.: Cloud droplet sedimentation, entrainment efficiency, and subtropical stratocumulus albedo, Geophysical Research Letters, 34, 2006GL027648, https://doi.org/10.1029/2006GL027648, 2007.

Buchard, V., Randles, C. A., Silva, A. M. da, Darmenov, A., Colarco, P. R., Govindaraju, R., Ferrare, R., Hair, J., Beyersdorf, A. J., Ziemba, L. D., and Yu, H.: The MERRA-2 Aerosol Reanalysis, 1980 Onward. Part II: Evaluation and Case Studies, Journal of Climate, 30, 6851–6872, https://doi.org/10.1175/JCLI-D-16-0613.1, 2017.

Caldwell, P., Bretherton, C. S., and Wood, R.: Mixed-Layer Budget Analysis of the Diurnal Cycle of Entrainment in Southeast Pacific Stratocumulus, Journal of the Atmospheric Sciences, 62, 3775–3791, https://doi.org/10.1175/JAS3561.1, 2005.

Change (IPCC), I. P. on C.: The Earth's Energy Budget, Climate Feedbacks and Climate Sensitivity, in: Climate Change 2021 – The Physical Science Basis: Working Group I Contribution to the Sixth Assessment Report of the Intergovernmental Panel on Climate Change, Cambridge University Press, 923–1054, 2023.

Chen, Y., Haywood, J., Wang, Y., Malavelle, F., Jordan, G., Partridge, D., Fieldsend, J., De Leeuw, J., Schmidt, A., Cho, N., Oreopoulos, L., Platnick, S., Grosvenor, D., Field, P., and Lohmann, U.: Machine learning reveals climate forcing from aerosols is dominated by increased cloud cover, Nat. Geosci., 15, 609–614, https://doi.org/10.1038/s41561-022-00991-6, 2022.

Chen, Y.-C., Christensen, M. W., Stephens, G. L., and Seinfeld, J. H.: Satellite-based estimate of global aerosol–cloud radiative forcing by marine warm clouds, Nature Geosci, 7, 643–646, https://doi.org/10.1038/ngeo2214, 2014.

Christensen, M. W. and Stephens, G. L.: Microphysical and macrophysical responses of marine stratocumulus polluted by underlying ships: Evidence of cloud deepening, J. Geophys. Res., 116, D03201, https://doi.org/10.1029/2010JD014638, 2011.

Coakley, J. A. and Walsh, C. D.: Limits to the Aerosol Indirect Radiative Effect Derived from Observations of Ship Tracks,

Journal of the Atmospheric Sciences, 59, 668–680, https://doi.org/10.1175/1520-0469(2002)059<0668:LTTAIR>2.0.CO;2, 2002.

Dagan, G., Koren, I., and Altaratz, O.: Competition between core and periphery-based processes in warm convective clouds – from invigoration to suppression, Atmospheric Chemistry and Physics, 15, 2749–2760, https://doi.org/10.5194/acp-15-2749-2015, 2015.

Duynkerke, P. G. and Hignett, P.: Simulation of Diurnal Variation in a Stratocumulus-capped Marine Boundary Layer during FIRE, Monthly Weather Review, 121, 3291–3300, https://doi.org/10.1175/1520-0493(1993)121<3291:SODVIA>2.0.CO;2, 1993.

Engström, A. and Ekman, A. M. L.: Impact of meteorological factors on the correlation between aerosol optical depth and cloud fraction: IMPACTS ON AEROSOL-CLOUD RELATIONSHIPS, Geophys. Res. Lett., 37, n/a-n/a, https://doi.org/10.1029/2010GL044361, 2010.

Feingold, G., Ghate, V. P., Russell, L. M., Blossey, P., Cantrell, W., Christensen, M. W., Diamond, M. S., Gettelman, A., Glassmeier, F., Gryspeerdt, E., Haywood, J., Hoffmann, F., Kaul, C. M., Lebsock, M., McComiskey, A. C., McCoy, D. T., Ming, Y., Mülmenstädt, J., Possner, A., Prabhakaran, P., Quinn, P. K., Schmidt, K. S., Shaw, R. A., Singer, C. E., Sorooshian, A., Toll, V., Wan, J. S., Wood, R., Yang, F., Zhang, J., and Zheng, X.: Physical science research needed to evaluate the viability and risks of marine cloud brightening, Sci. Adv., 10, eadi8594, https://doi.org/10.1126/sciadv.adi8594, 2024.

Fons, E., Runge, J., Neubauer, D., and Lohmann, U.: Stratocumulus adjustments to aerosol perturbations disentangled with a causal approach, npj Clim Atmos Sci, 6, 130, https://doi.org/10.1038/s41612-023-00452-w, 2023.

George, R. C. and Wood, R.: Subseasonal variability of low cloud radiative properties over the southeast Pacific Ocean, Atmos. Chem. Phys., 10, 4047–4063, https://doi.org/10.5194/acp-10-4047-2010, 2010.

Ghosh, S., Osborne, S., and Smith, M. H.: On the importance of cumulus penetration on the microphysical and optical properties of stratocumulus clouds, Atmospheric Chemistry and Physics, 5, 755–765, https://doi.org/10.5194/acp-5-755-2005, 2005.

Glassmeier, F., Hoffmann, F., Johnson, J. S., Yamaguchi, T., Carslaw, K. S., and Feingold, G.: Aerosol-cloud-climate cooling overestimated by ship-track data, Science, 371, 485–489, https://doi.org/10.1126/science.abd3980, 2021.

Grosvenor, D. P., Sourdeval, O., Zuidema, P., Ackerman, A., Alexandrov, M. D., Bennartz, R., Boers, R., Cairns, B., Chiu, J. C., Christensen, M., Deneke, H., Diamond, M., Feingold, G., Fridlind, A., Hünerbein, A., Knist, C., Kollias, P., Marshak, A., McCoy, D., Merk, D., Painemal, D., Rausch, J., Rosenfeld, D., Russchenberg, H., Seifert, P., Sinclair, K., Stier, P., van Diedenhoven, B., Wendisch, M., Werner, F., Wood, R., Zhang, Z., and Quaas, J.: Remote Sensing of Droplet Number Concentration in Warm Clouds: A Review of the Current State of Knowledge and Perspectives, Reviews of Geophysics, 56, 409–453, https://doi.org/10.1029/2017RG000593, 2018.

Gryspeerdt, E., Goren, T., Sourdeval, O., Quaas, J., Mülmenstädt, J., Dipu, S., Unglaub, C., Gettelman, A., and Christensen, M.: Constraining the aerosol influence on cloud liquid water path, Atmos. Chem. Phys., 19, 5331–5347, https://doi.org/10.5194/acp-19-5331-2019, 2019.

https://doi.org/10.5194/egusphere-2024-3601
Preprint. Discussion started: 16 December 2024

Gryspeerdt, E., Goren, T., and Smith, T. W. P.: Observing the timescales of aerosol–cloud interactions in snapshot satellite images, Atmos. Chem. Phys., 21, 6093–6109, https://doi.org/10.5194/acp-21-6093-2021, 2021.

Gryspeerdt, E., Glassmeier, F., Feingold, G., Hoffmann, F., and Murray-Watson, R. J.: Observing short-timescale cloud development to constrain aerosol–cloud interactions, Atmos. Chem. Phys., 22, 11727–11738, https://doi.org/10.5194/acp-22-11727-2022, 2022a.

Gryspeerdt, E., McCoy, D. T., Crosbie, E., Moore, R. H., Nott, G. J., Painemal, D., Small-Griswold, J., Sorooshian, A., and Ziemba, L.: The impact of sampling strategy on the cloud droplet number concentration estimated from satellite data, Atmos. Meas. Tech., 15, 3875–3892, https://doi.org/10.5194/amt-15-3875-2022, 2022b.

Han, Q., Rossow, W. B., Zeng, J., and Welch, R.: Three Different Behaviors of Liquid Water Path of Water Clouds in Aerosol–Cloud Interactions, Journal of the Atmospheric Sciences, 59, 726–735, https://doi.org/10.1175/1520-0469(2002)059<0726:TDBOLW>2.0.CO;2, 2002.

Hersbach, H., Bell, B., Berrisford, P., Hirahara, S., Horányi, A., Muñoz-Sabater, J., Nicolas, J., Peubey, C., Radu, R., Schepers, D., Simmons, A., Soci, C., Abdalla, S., Abellan, X., Balsamo, G., Bechtold, P., Biavati, G., Bidlot, J., Bonavita, M., De Chiara, G., Dahlgren, P., Dee, D., Diamantakis, M., Dragani, R., Flemming, J., Forbes, R., Fuentes, M., Geer, A., Haimberger, L., Healy, S., Hogan, R. J., Hólm, E., Janisková, M., Keeley, S., Laloyaux, P., Lopez, P., Lupu, C., Radnoti, G., de Rosnay, P., Rozum, I., Vamborg, F., Villaume, S., and Thépaut, J.-N.: The ERA5 global reanalysis, Quarterly Journal of the Royal Meteorological Society, 146, 1999–2049, https://doi.org/10.1002/qj.3803, 2020.

Hu, Y., Lu, X., Zhai, P.-W., Hostetler, C. A., Hair, J. W., Cairns, B., Sun, W., Stamnes, S., Omar, A., Baize, R., Videen, G., Mace, J., McCoy, D. T., McCoy, I. L., and Wood, R.: Liquid Phase Cloud Microphysical Property Estimates From CALIPSO Measurements, Front. Remote Sens., 2, https://doi.org/10.3389/frsen.2021.724615, 2021.

Huffman, G. J., Bolvin, D. T., Braithwaite, D., Hsu, K.-L., Joyce, R. J., Kidd, C., Nelkin, E. J., Sorooshian, S., Stocker, E. F., Tan, J., Wolff, D. B., and Xie, P.: Integrated Multi-satellite Retrievals for the Global Precipitation Measurement (GPM) Mission (IMERG), in: Satellite Precipitation Measurement: Volume 1, edited by: Levizzani, V., Kidd, C., Kirschbaum, D. B., Kummerow, C. D., Nakamura, K., and Turk, F. J., Springer International Publishing, Cham, 343–353, https://doi.org/10.1007/978-3-030-24568-9_19, 2020.

Jian, B., Li, J., Wang, G., Zhao, Y., Li, Y., Wang, J., Zhang, M., and Huang, J.: Evaluation of the CMIP6 marine subtropical stratocumulus cloud albedo and its controlling factors, Atmos. Chem. Phys., 21, 9809–9828, https://doi.org/10.5194/acp-21-9809-2021, 2021.

Jiang, X., Su, H., Jiang, J. H., Neelin, J. D., Wu, L., Tsushima, Y., and Elsaesser, G.: Muted extratropical low cloud seasonal cycle is closely linked to underestimated climate sensitivity in models, Nat Commun, 14, 5586, https://doi.org/10.1038/s41467-023-41360-0, 2023.

Kang, L., Marchand, R., and Smith, W.: Evaluation of MODIS and Himawari-8 Low Clouds Retrievals Over the Southern Ocean With In Situ Measurements From the SOCRATES Campaign, Earth and Space Science, 8, https://doi.org/10.1029/2020EA001397, 2021.

https://doi.org/10.5194/egusphere-2024-3601
Preprint. Discussion started: 16 December 2024

Kaufman, Y. J., Koren, I., Remer, L. A., Rosenfeld, D., and Rudich, Y.: The effect of smoke, dust, and pollution aerosol on shallow cloud development over the Atlantic Ocean, Proc. Natl. Acad. Sci. U.S.A., 102, 11207–11212, https://doi.org/10.1073/pnas.0505191102, 2005.

Kazil, J., Yamaguchi, T., and Feingold, G.: Mesoscale organization, entrainment, and the properties of a closed-cell stratocumulus cloud, Journal of Advances in Modeling Earth Systems, 9, 2214–2229, https://doi.org/10.1002/2017MS001072, 2017.

Klein, S. A. and Hartmann, D. L.: The Seasonal Cycle of Low Stratiform Clouds, Journal of Climate, 6, 1587–1606, https://doi.org/10.1175/1520-0442(1993)006<1587:TSCOLS>2.0.CO;2, 1993.

Koren, I., Dagan, G., and Altaratz, O.: From aerosol-limited to invigoration of warm convective clouds, Science, 344, 1143–1146, https://doi.org/10.1126/science.1252595, 2014.

Lee, S. S., Penner, J. E., and Saleeby, S. M.: Aerosol effects on liquid-water path of thin stratocumulus clouds, J. Geophys. Res., 114, D07204, https://doi.org/10.1029/2008JD010513, 2009.

Li, J., Jian, B., Huang, J., Hu, Y., Zhao, C., Kawamoto, K., Liao, S., and Wu, M.: Long-term variation of cloud droplet number concentrations from space-based Lidar, Remote Sensing of Environment, 213, 144–161, https://doi.org/10.1016/j.rse.2018.05.011, 2018.

Li, X., O, S., Wang, N., Liu, lichen, and Huang, Y.: Evaluation of the GPM IMERG V06 products for light rain over Mainland China, Atmospheric Research, 253, 105510, https://doi.org/10.1016/j.atmosres.2021.105510, 2021.

Luo, T., Wang, Z., Zhang, D., and Chen, B.: Marine boundary layer structure as observed by A-train satellites, Atmospheric Chemistry and Physics, 16, 5891–5903, https://doi.org/10.5194/acp-16-5891-2016, 2016.

Martin, G. M., Johnson, D. W., and Spice, A.: The Measurement and Parameterization of Effective Radius of Droplets in Warm Stratocumulus Clouds, Journal of the Atmospheric Sciences, 51, 1823–1842, https://doi.org/10.1175/1520-0469(1994)051<1823:TMAPOE>2.0.CO;2, 1994.

Martin, G. M., Johnson, D. W., Rogers, D. P., Jonas, P. R., Minnis, P., and Hegg, D. A.: Observations of the Interaction between Cumulus Clouds and Warm Stratocumulus Clouds in the Marine Boundary Layer during ASTEX, Journal of the Atmospheric Sciences, 52, 2902–2922, https://doi.org/10.1175/1520-0469(1995)052<2902:OOTIBC>2.0.CO;2, 1995.

McCoy, D. T., Burrows, S. M., Wood, R., Grosvenor, D. P., Elliott, S. M., Ma, P.-L., Rasch, P. J., and Hartmann, D. L.: Natural aerosols explain seasonal and spatial patterns of Southern Ocean cloud albedo, Sci. Adv., 1, e1500157, https://doi.org/10.1126/sciadv.1500157, 2015.

McCoy, D. T., Bender, F. A.-M., Grosvenor, D. P., Mohrmann, J. K., Hartmann, D. L., Wood, R., and Field, P. R.: Predicting decadal trends in cloud droplet number concentration using reanalysis and satellite data, Atmos. Chem. Phys., 18, 2035–2047, https://doi.org/10.5194/acp-18-2035-2018, 2018.

Mechoso, C. R., Wood, R., Weller, R., Bretherton, C. S., Clarke, A. D., Coe, H., Fairall, C., Farrar, J. T., Feingold, G., Garreaud, R., Grados, C., McWilliams, J., Szoeke, S. P. de, Yuter, S. E., and Zuidema, P.: Ocean–Cloud–Atmosphere–Land Interactions in the Southeastern Pacific: The VOCALS Program, Bulletin of the American Meteorological Society, 95, 357–375,

https://doi.org/10.1175/BAMS-D-11-00246.1, 2014.

Michibata, T., Suzuki, K., Sato, Y., and Takemura, T.: The source of discrepancies in aerosol–cloud–precipitation interactions between GCM and A-Train retrievals, Atmos. Chem. Phys., 16, 15413–15424, https://doi.org/10.5194/acp-16-15413-2016, 2016.

Miller, M. A., Jensen, M. P., and Clothiaux, E. E.: Diurnal Cloud and Thermodynamic Variations in the Stratocumulus Transition Regime: A Case Study Using In Situ and Remote Sensors, Journal of the Atmospheric Sciences, 55, 2294–2310, https://doi.org/10.1175/1520-0469(1998)055<2294:DCATVI>2.0.CO;2, 1998.

Miller, S. D., Rogers, M. A., Haynes, J. M., Sengupta, M., and Heidinger, A. K.: Short-term solar irradiance forecasting via satellite/model coupling, Solar Energy, 168, 102–117, https://doi.org/10.1016/j.solener.2017.11.049, 2018.

Min, Q., Joseph, E., Lin, Y., Min, L., Yin, B., Daum, P. H., Kleinman, L. I., Wang, J., and Lee, Y.-N.: Comparison of MODIS cloud microphysical properties with in-situ measurements over the Southeast Pacific, Atmospheric Chemistry and Physics, 12, 11261–11273, https://doi.org/10.5194/acp-12-11261-2012, 2012.

Minnis, P., Sun-Mack, S., Chen, Y., Chang, F.-L., Yost, C. R., Smith, W. L., Heck, P. W., Arduini, R. F., Bedka, S. T., Yi, Y., Hong, G., Jin, Z., Painemal, D., Palikonda, R., Scarino, B. R., Spangenberg, D. A., Smith, R. A., Trepte, Q. Z., Yang, P., and Xie, Y.: CERES MODIS Cloud Product Retrievals for Edition 4—Part I: Algorithm Changes, IEEE Transactions on Geoscience and Remote Sensing, 59, 2744–2780, https://doi.org/10.1109/TGRS.2020.3008866, 2021.

NASA/LARC/SD/ASDC: SatCORPS CERES GEO Edition 4 Himawari-8 Northern Hemisphere Version 1.2, 2018a.

NASA/LARC/SD/ASDC: SatCORPS CERES GEO Edition 4 Himawari-8 Southern Hemisphere Version 1.2, 2018b.

Painemal, D. and Zuidema, P.: Assessment of MODIS cloud effective radius and optical thickness retrievals over the Southeast Pacific with VOCALS-REx in situ measurements, Journal of Geophysical Research: Atmospheres, 116, https://doi.org/10.1029/2011JD016155, 2011.

Painemal, D., Minnis, P., and O'Neill, L.: The Diurnal Cycle of Cloud-Top Height and Cloud Cover over the Southeastern Pacific as Observed by GOES-10, Journal of the Atmospheric Sciences, 70, 2393–2408, https://doi.org/10.1175/JAS-D-12-0325.1, 2013.

Painemal, D., Xu, K., Palikonda, R., and Minnis, P.: Entrainment rate diurnal cycle in marine stratiform clouds estimated from geostationary satellite retrievals and a meteorological forecast model, Geophysical Research Letters, 44, 7482–7489, https://doi.org/10.1002/2017GL074481, 2017.

Petters, J. L., Harrington, J. Y., and Clothiaux, E. E.: Radiative–Dynamical Feedbacks in Low Liquid Water Path Stratiform Clouds, https://doi.org/10.1175/JAS-D-11-0169.1, 2012.

Qiu, S., Zheng, X., Painemal, D., Terai, C. R., and Zhou, X.: Daytime variation in the aerosol indirect effect for warm marine boundary layer clouds in the eastern North Atlantic, Atmospheric Chemistry and Physics, 24, 2913–2935, https://doi.org/10.5194/acp-24-2913-2024, 2024.

Qu, X., Hall, A., Klein, S. A., and DeAngelis, A. M.: Positive tropical marine low-cloud cover feedback inferred from cloud-controlling factors, Geophys. Res. Lett., 42, 7767–7775, https://doi.org/10.1002/2015GL065627, 2015.

https://doi.org/10.5194/egusphere-2024-3601
Preprint. Discussion started: 16 December 2024

Quaas, J., Boucher, O., and Lohmann, U.: Constraining the total aerosol indirect effect in the LMDZ and ECHAM4 GCMs using MODIS satellite data, Atmospheric Chemistry and Physics, 6, 947–955, https://doi.org/10.5194/acp-6-947-2006, 2006.

Rahu, J., Trofimov, H., Post, P., and Toll, V.: Diurnal Evolution of Cloud Water Responses to Aerosols, JGR Atmospheres, 127, https://doi.org/10.1029/2021JD035091, 2022.

Rogers, D. P., Yang, X., Norris, P. M., Johnson, D. W., Martin, G. M., Friehe, C. A., and Berger, B. W.: Diurnal Evolution of the Cloud-Topped Marine Boundary Layer. Part I: Nocturnal Stratocumulus Development, Journal of the Atmospheric Sciences, 52, 2953–2966, https://doi.org/10.1175/1520-0469(1995)052<2953:DEOTCT>2.0.CO;2, 1995.

Rosenfeld, D., Wang, H., and Rasch, P. J.: The roles of cloud drop effective radius and LWP in determining rain properties in marine stratocumulus, Geophysical Research Letters, 39, https://doi.org/10.1029/2012GL052028, 2012.

Rosenfeld, D., Zhu, Y., Wang, M., Zheng, Y., Goren, T., and Yu, S.: Aerosol-driven droplet concentrations dominate coverage and water of oceanic low-level clouds, Science, 363, eaav0566, https://doi.org/10.1126/science.aav0566, 2019.

Rosenfeld, D., Kokhanovsky, A., Goren, T., Gryspeerdt, E., Hasekamp, O., Jia, H., Lopatin, A., Quaas, J., Pan, Z., and Sourdeval, O.: Frontiers in Satellite-Based Estimates of Cloud-Mediated Aerosol Forcing, Reviews of Geophysics, 61, e2022RG000799, https://doi.org/10.1029/2022RG000799, 2023.

Slingo, A., Nicholls, S., and Schmetz, J.: Aircraft observations of marine stratocumulus during JASIN, Quart J Royal Meteoro Soc, 108, 833–856, https://doi.org/10.1002/qj.49710845807, 1982.

Small, J. D., Chuang, P. Y., Feingold, G., and Jiang, H.: Can aerosol decrease cloud lifetime?, Geophys. Res. Lett., 36, L16806, https://doi.org/10.1029/2009GL038888, 2009.

Smalley, K. M., Lebsock, M. D., and Eastman, R.: Diurnal Patterns in the Observed Cloud Liquid Water Path Response to Droplet Number Perturbations, Geophysical Research Letters, 51, e2023GL107323, https://doi.org/10.1029/2023GL107323, 2024.

Stevens, B.: Cloud transitions and decoupling in shear-free stratocumulus-topped boundary layers, Geophysical Research Letters, 27, 2557–2560, https://doi.org/10.1029/1999GL011257, 2000.

Toll, V., Christensen, M., Quaas, J., and Bellouin, N.: Weak average liquid-cloud-water response to anthropogenic aerosols, Nature, 572, 51–55, https://doi.org/10.1038/s41586-019-1423-9, 2019.

Trepte, Q. Z., Minnis, P., Sun-Mack, S., Yost, C. R., Chen, Y., Jin, Z., Hong, G., Chang, F.-L., Smith, W. L., Bedka, K. M., and Chee, T. L.: Global Cloud Detection for CERES Edition 4 Using Terra and Aqua MODIS Data, IEEE Transactions on Geoscience and Remote Sensing, 57, 9410–9449, https://doi.org/10.1109/TGRS.2019.2926620, 2019.

Trofimov, H., Bellouin, N., and Toll, V.: Large-Scale Industrial Cloud Perturbations Confirm Bidirectional Cloud Water Responses to Anthropogenic Aerosols, JGR Atmospheres, 125, https://doi.org/10.1029/2020JD032575, 2020.

Twomey, S.: The nuclei of natural cloud formation part II: The supersaturation in natural clouds and the variation of cloud droplet concentration, Geofisica Pura e Applicata, 43, 243–249, https://doi.org/10.1007/BF01993560, 1959.

Twomey, S.: The Influence of Pollution on the Shortwave Albedo of Clouds, Journal of the Atmospheric Sciences, 34, 1149–1152, https://doi.org/10.1175/1520-0469(1977)034<1149:TIOPOT>2.0.CO;2, 1977.

https://doi.org/10.5194/egusphere-2024-3601
Preprint. Discussion started: 16 December 2024

Marine Low Clouds : Radiation, Turbulence, and Forecasting:

Wilcox, E. M.: Stratocumulus cloud thickening beneath layers of absorbing smoke aerosol, Atmospheric Chemistry and Physics, 10, 11769–11777, https://doi.org/10.5194/acp-10-11769-2010, 2010.

Wood, R., Bretherton, C. S., and Hartmann, D. L.: Diurnal cycle of liquid water path over the subtropical and tropical oceans: DIURNAL CYCLE OF LIQUID WATER PATH, Geophys. Res. Lett., 29, 7-1-7–4, https://doi.org/10.1029/2002GL015371, 2002.

Zhang, J. and Feingold, G.: Distinct regional meteorological influences on low-cloud albedo susceptibility over global marine stratocumulus regions, Atmospheric Chemistry and Physics, 23, 1073–1090, https://doi.org/10.5194/acp-23-1073-2023, 2023.

Zhang, J., Chen, Y.-S., Yamaguchi, T., and Feingold, G.: Cloud water adjustments to aerosol perturbations are buffered by solar heating in non-precipitating marine stratocumuli, EGUsphere, 1–27, https://doi.org/10.5194/egusphere-2024-1021, 2024.

Zhang, X., Wang, H., Che, H.-Z., Tan, S.-C., Yao, X.-P., Peng, Y., and Shi, G.-Y.: Radiative forcing of the aerosol-cloud interaction in seriously polluted East China and East China Sea, Atmospheric Research, 252, 105405, https://doi.org/10.1016/j.atmosres.2020.105405, 2021.

Zheng, Y., Rosenfeld, D., and Li, Z.: Estimating the Decoupling Degree of Subtropical Marine Stratocumulus Decks From Satellite, Geophysical Research Letters, 45, 12,560-12,568, https://doi.org/10.1029/2018GL078382, 2018.